Cone metrics: a new tool for the intercomparison of scatterometer records

Maria Belmonte Rivas, Ad Stoffelen, Jeroen Verspeek, Anton Verhoef, Xavier Neyt and Craig Anderson

***Abstract*— With an eye on the generation of a long-term climate record of ocean winds, soil moisture and sea ice extents across the C-band ERS and ASCAT scatterometer spans, a new calibration tool termed cone metrics has been developed. The new method is based on monitoring changes in the location and shape of the surface of maximum density of ocean backscatter measurements, also known as "the wind cone". The cone metrics technique complements established calibration approaches, such as rain forest and NWP ocean calibration, through the characterization of linear as well as non-linear beam offsets, the latter via wind cone deformations. Given instrument evolution, proven stability and the monitoring by transponders, we take ASCAT-A data over 2013 as absolute calibration reference. This paper describes the new method and its application as inter-calibration tool in the context of the reprocessing activities for ERS-1 and ERS-2. Cone metrics succeeds at establishing the linear and non-linear corrections necessary to homogenize the ASCAT and ERS C-band records down to 0.05 dB.**

***Index Terms*—Radar signal processing, calibration, antenna radiation pattern.**

I. Introduction

LONG-TERM climate records of proven homogeneity are fundamental to study climate change and variability. The combination of existing C-band and Ku-band scatterometer data archives into a single climate data record (CDR) shall provide an invaluable registry of ocean surface vector winds, soil moisture and sea ice extents dating from 1991 to present date. While the homogenization of the C-band and Ku-band scatterometer records remains a challenge, mainly because of their different radar physics [1] [2], the homogenization of the C-band record formed by the Advanced Scatterometer (ASCAT) data collected on Metop-A [3], and the Active Microwave Instrument (AMI) data collected on the European Remote Sensing ERS-1 and ERS-2 [4] is already obtainable.

The Global Climate Observing System (GCOS) program defines guidelines for the provision of satellite-based essential climate variables (ECVs), prescribing a stability requirement of 0.1 m/s per decade for the provision of ocean surface winds [5], which translates into a relative beam stability of 0.1 dB at C-band. Historically, the stability of scatterometer data has relied on vicarious calibration techniques that depend on external references such as the backscatter from the tropical rain forest [6], ground transponder data [7], or the ocean winds from a Numerical Weather Prediction (NWP) model [8]. The calibration accuracy obtained by the rain forest method, which is limited by the intrinsic variability of the rain forest backscatter, is estimated to be ±0.15 dB [9]. The calibration accuracy obtained by ground transponders is estimated to be ±0.15 dB [7], and that from ocean calibration, which is limited by uncertainties in the NWP model wind distribution, is estimated to be on the order of 0.1-0.2 dB. It is important to note that all of these calibration techniques, which essentially determine any antenna gain offsets that may occur due to uncertainties in the radar link budget, operate under the assumption of linear calibration, that is, the radar backscatter σ^0_{obs} measured by an instrument is related to its true value σ^0 by an unknown calibration constant δ as:

$$\sigma^0_{obs} = (1+\delta)\cdot\sigma^0 \quad (1)$$

Which takes the form of a constant beam bias in dB space:

$$\sigma^0_{obs,dB} = \sigma^0_{dB} + \delta_{dB} \quad (2)$$

Where $\delta_{dB} = 10\log_{10}(1+\delta)$. Beam calibration non-linearities, which arise as soon as the scatterometer beam offset δ_{dB} varies with backscatter level, have been detected between the ERS and ASCAT records [10]. These non-linearities may have diverse instrumental origins, such as the antenna noise floor estimation, the non-linear corrections in analogue-to-digital conversion, pointing uncertainties, and other characterization and processing anomalies that may not be quantitatively obtainable due to lack of documentation. Beam non-linearities entail complicated biases that none of the methods above consider in their formulations, and are likely to result in irreversible non-linear wind retrieval biases. The focus of this work lies on the development of a novel calibration method (Section II) capable of characterizing and correcting for non-linear beam biases (Section III) in an attempt towards the homogenization of the C-band ERS and ASCAT scatterometer backscatter records.

Manuscript submitted on June 24th 2016 for review. This work was supported by the European Space Agency (ESA) Scatterometer Instrument Competence Center (SCIROCCO project).

M. Belmonte Rivas is with the Royal Netherlands Meteorology Institute in de Bilt, The Netherlands, under authorized stay at the Institute of Marine Sciences (CSIC-ICM) in Barcelona, Spain (e-mail: belmonte@knmi.nl, belmonte@icm.csic.es). A. Stoffelen, J. Verspeek and A. Verhoef, are with the Royal Netherlands Meteorology Institute in de Bilt, The Netherlands (e-mails: ad.stoffelen@knmi.nl, verspeek@knmi.nl, verhoefa@knmi.nl). C. Anderson is with the European Organization for the Exploitation of Meteorological Satellites (EUMETSAT) in Darmstadt, Germany (e-mail: craig.anderson@eumetsat.int). X. Neyt is with the Royal Military Academy in Brussels, Belgium (Xavier.Neyt@elec.rma.ac.be).

II. Cone Metrics

Cone metrics are based on monitoring changes in the distribution of ocean backscatter points in the scatterometer measurement space. Both the ASCAT and ERS scatterometers are C-band radars holding three vertically-polarized fan-beam antennas oriented at 45°, 90° and 135° with respect to the satellite track (Fig.1). Processing of the return echoes resolves the reflected power into separate spatial nodes across the swath. Every node or wind vector cell (WVC) across the swath is sequentially illuminated by the fore, mid and aft antennas to form a backscatter triplet in a three-dimensional space. The observation angles that correspond to each WVC are outlined in Table I. Note that the ASCAT instrument illuminates the surface at slightly larger incidence angles than ERS, and over a larger swath (using 25 km grids, the ERS antennas illuminate 19 nodes on the right side only, whereas ASCAT illuminates 21 nodes on both sides). Another disparity between these records relates to their slightly different local descending solar equatorial times: 10:30 am for ERS and 9:30 am for ASCAT.

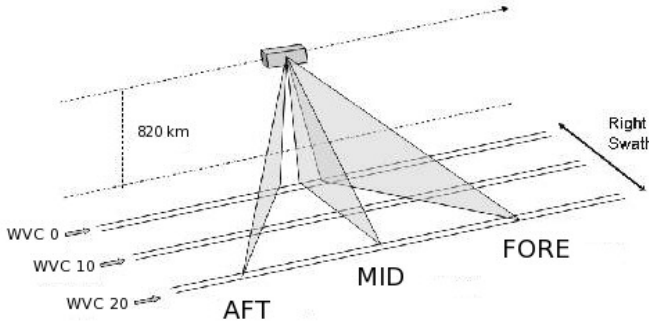

Fig. 1. Observation geometry for the ASCAT and ERS scatterometers. The swath is divided into Wind Vector Cells (WVCs) separated as a function of distance from the satellite track. As the satellite passes overhead, each WVC is illuminated first by the fore, then mid, then aft antennas, resulting in a backscatter triplet.

TABLE I
Scatterometer Nodes and Mean Observation Angles

ASCAT WVC #	INCIDENCE {mid, fore/aft}	ERS WVC #	INCIDENCE {mid, fore/aft}	X_{low} (dB)
		0	18.0°, 24.8°	-13
		1	19.8°, 27.2°	-15
		2	21.7°, 29.6°	-17
		3	23.5°, 31.8°	-19
		4	25.2°, 34.0°	-21
0	27.5°, 36.8°	5	26.9°, 36.1°	-25
1	29.1°, 38.7°	*6*	28.6°, 38.1°	-27
2	30.7°, 40.5°	*7*	30.2°, 40.0°	-28
3	32.2°, 42.3°	*8*	31.8°, 41.8°	-29
4	33.6°, 43.9°	*9*	33.4°, 43.6°	-30
5	35.1°, 45.6°	*10*	34.9°, 45.3°	-31
6	36.5°, 47.1°	*11*	36.3°, 46.9°	-32
7	37.8°, 48.6°	*12*	37.7°, 48.5°	-33
8	39.1°, 50.1°	*13*	39.1°, 49.9°	-33
9	40.3°, 51.5°	*14*	40.5°, 51.4°	-34
10	41.7°, 52.8°	*15*	41.8°, 52.8°	-34
11	42.9°, 54.0°	*16*	43.0°, 54.1°	-35
12	44.1°, 55.3°	*17*	44.2°, 55.3°	-35
13	45.2°, 56.5°	*18*	45.4°, 56.5°	-36
14	46.3°, 57.6°			-36
15	47.4°, 58.7°			-37
16	48.5°, 59.8°			-37
17	49.5°, 60.8°			-38
18	50.5°, 61.8°			-38
19	51.4°, 62.7°			-38
20	52.4°, 63.6°			-39

Incidence angles are averaged over the orbit of the scatterometer.

The backscatter triplets collected at C-band over the ocean are distributed along a double-folded conical surface in the ASCAT (ERS) measurement space, also known as the "wind cone" [11]. The surface of the wind cone is typically parameterized in terms of surface wind speed and direction, enabling the retrieval of the ocean wind vector. The working principle of cone metrics states that the ocean backscatter triplets collected under identical observation angles must

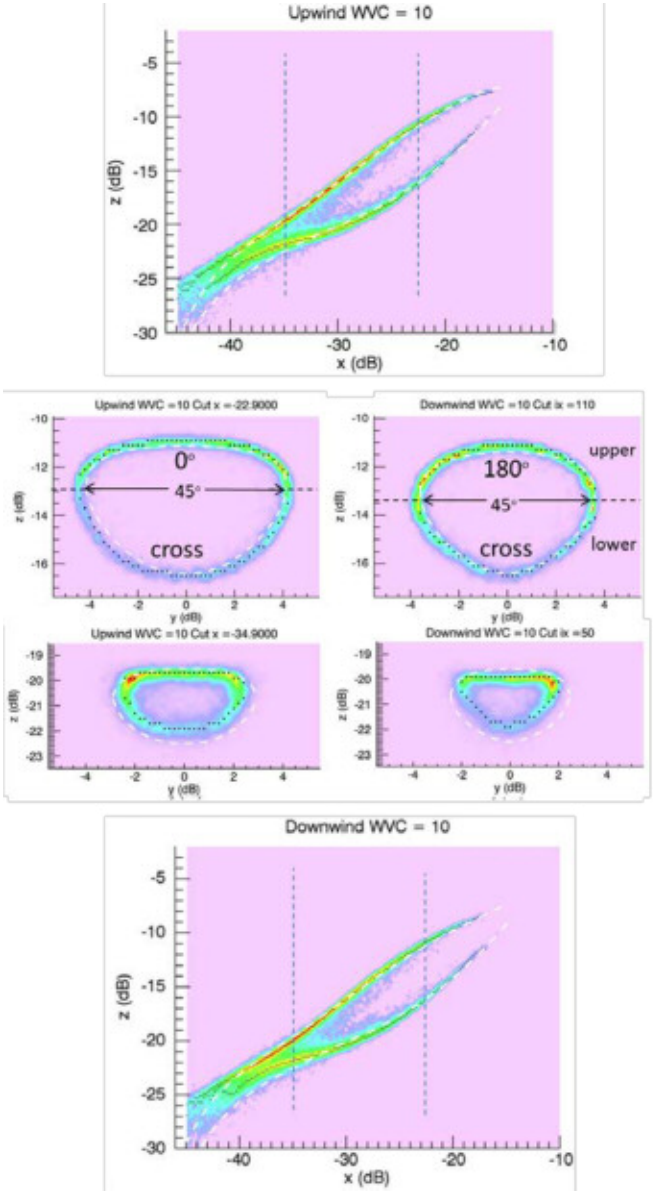

Fig. 2. The surface of maximum backscatter density (black dots) determined from ASCAT-A histograms (color scaled) of backscatter triplets in {x,y,z} space for WVC 10. The top (bottom) panel shows a section of the upwind (downwind) cone across the symmetry y = 0 plane. The middle panels show sections of the upwind (left) and downwind (right) cones across two different x = constant planes (indicated by dashed lines in top and bottom panels). The CMOD6 model function is overlaid in dashed white for reference. Also shown are the approximate locations of the upwind (0°), downwind (180°) and crosswind (90°) points.

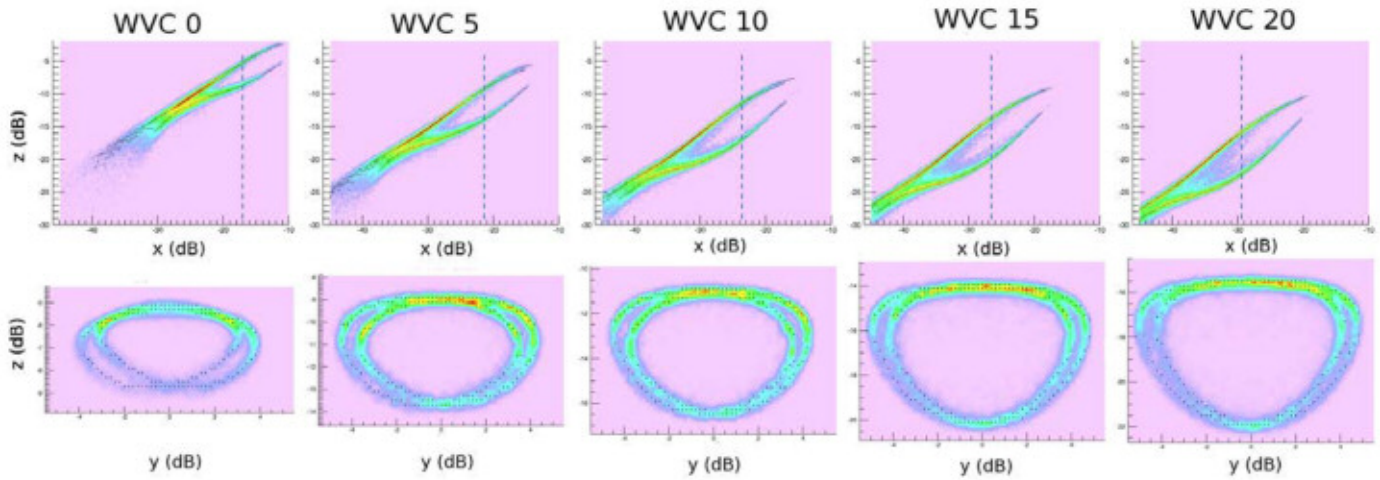

Fig. 3. The surface of maximum backscatter density (black dots) from ASCAT-A histograms (color scaled) over 2013. The top panels show sections of the wind cone across the symmetry y = 0 plane for WVC numbers 0, 5, 10, 15 and 20. The bottom panels show sections of the wind cones across a certain x = constant plane (indicated by dashed lines in the top panels).

conform to the same double-folded conical surface, regardless of weather or climate related changes in the underlying wind distribution. Inconsistencies between the backscatter distributions observed by different instruments over different periods may therefore be attributed to relative beam calibration biases (which will shift the location of the wind cone) or beam non-linearities (which will cause the wind cone to deform). When unchecked, shifts and deformations will pull the measurement cone away from the geophysical model function (GMF) used for wind retrieval, affecting the ensuing wind CDR.

A. The wind cone

The wind cone is defined as the surface of maximum density of ocean backscatter points in the three-dimensional space formed by the scatterometer fore, aft and mid beam measurements. In cone metrics, the maximum density surface results from the analysis of the 3D histograms of backscatter data accumulated over a certain period (e.g., one month or one year) using 0.2 dB bin heights. To limit our analysis to ocean points, land and sea ice observations are screened out, as well as poor quality wind retrievals (i.e. quality flagged). In order to take advantage of the nominal cone invariance after fore and aft beam reversals, the original measurements are transformed into a new {x,y,z} frame of coordinates as:

$$\begin{aligned} x &= (\sigma^0_{fore} + \sigma^0_{aft})/\sqrt{2} \\ y &= (\sigma^0_{fore} - \sigma^0_{aft})/\sqrt{2} \\ z &= \sigma^0_{mid} \end{aligned} \tag{3}$$

such that the symmetry plane of the wind cone lies on y = 0.

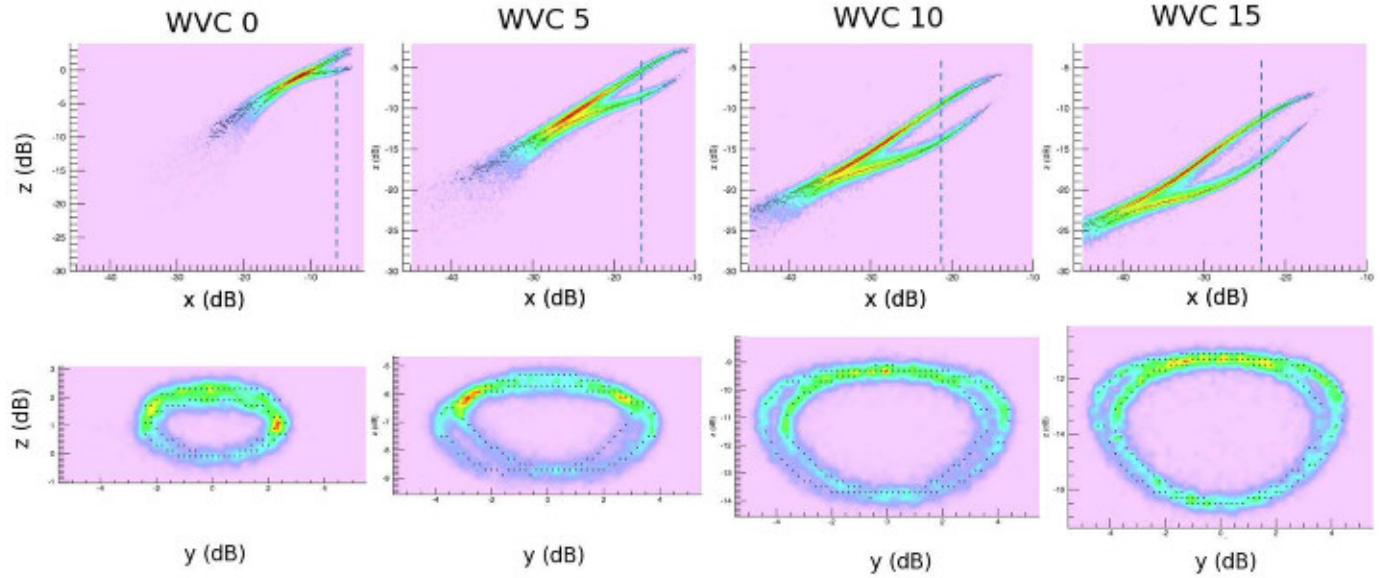

Fig. 4. The surface of maximum backscatter density (black dots) from ERS-2 histograms (color scaled) over 1997. The top panels show sections of the wind cone across the symmetry y = 0 plane for WVC numbers 0, 5, 10 and 15. The bottom panels show sections of the wind cones across a certain x = constant plane (indicated by dashed lines in the top panels). Note that the ERS WVC 15 cone in this figure corresponds to the ASCAT WVC 10 cone in Figure 3 (see Table I).

Because of the double-folded nature of the wind cone, and in order to ease the detection of single-valued maxima in the backscatter distributions, the original 3D histograms are split into separate Z(x,y) branch surfaces for upwind and downwind conditions using collocated model wind directions. The winds blowing towards the mid beam (with relative azimuths < |90|°) define the upwind cone, whereas winds blowing away from the mid beam will define the downwind cone (see left and right middle panels in Fig. 2). The upwind and downwind cones are connected roughly along the crosswind line defined by ±90° in relative wind azimuth, and reach their widest lateral extent (on the y-axis) 45° away from the crosswind line. These 45° midpoints are chosen to separate the upper and lower branches of the upwind and downwind cones (see Fig. 2), so that four well-defined and single-valued surfaces result: two for the upper and lower branches of the upwind cone (Z_{upUP} and Z_{loUP}) and another two for the upper and lower branches of the downwind cone (Z_{upDN} and Z_{loDN}).

A peak detection algorithm is run across the x and y dimensions of the now split 3D histograms to detect the single-valued z at which the histogram reaches its maximum density, so to generate the $Z_j(x,y)$ surface that corresponds to each branch (j=1,…4). The procedure is repeated for each node, so that a bundle of WVC-dependent wind cones emerges from every dataset (see Figs. 3-4 for a depiction of sample ASCAT and ERS wind cones). Note that at low backscatter, the maximum density points no longer conform to a smooth surface, because the separation of cone branches in terms of relative wind azimuths is made difficult by weak statistics and low wind direction sensitivity. In order to exclude uncertainty in the wind cone definition, we introduce an array of node-dependent thresholds on the x-coordinate, roughly corresponding to backscatter at 5 m/s, below which maximum density surfaces are not defined (see last column on Table I).

B. Linear beam offsets and residuals

Suppose that a reference wind cone $Z_j^{ref}(x,y)$ is established using a reference dataset, i.e., the backscatter collected by a stable instrument over a given period (such as from ASCAT-A over 2013, which we take as reference due to its superior stability and absolute calibration from transponder data [7]). Under the assumption of linear calibration [see Eq. (2)], every other wind cone may be related to this reference cone through simple solid body translations.

The relative linear beam offset between two datasets is determined by finding the $\{\Delta x, \Delta y\}$ combination of horizontal cone shifts that minimizes the root-mean-square (RMS) of the branch residuals:

$$J(\Delta x, \Delta y) = RMS[res_j(x, y; \Delta x, \Delta y)] \quad (4)$$

Where branch residuals are defined as:

$$res_j(x, y; \Delta x, \Delta y) = Z_j(x + \Delta x, y + \Delta y) - Z_j^{ref}(x, y) \quad (5)$$

And the subindex *j* stands for the four separate cone branches (upper upwind, upper downwind, lower upwind and lower downwind). The RMS residual $J(\Delta x,\Delta y)$ to the reference cone is calculated over the four $Z_j(x,y)$ surfaces defined over [-45,0] dB in x and [-5.5,5.5] dB in y. The numerical search for the optimal combination of horizontal cone shifts $\{\Delta x_{min}, \Delta y_{min}\}$ that minimizes the RMS difference to the reference cone sweeps a range of ±2 dB in both Δx and Δy in steps of 0.02 dB. The optimal combination of horizontal cone shifts $\{\Delta x_{min}, \Delta y_{min}\}$ also solves for the vertical cone shift Δz:

$$\Delta z = mean[res_j(x, y; \Delta x_{\min}, \Delta y_{\min})] \quad (6)$$

That is, having minimized the part of the RMS difference that depends on horizontal shift, one guarantees that the surfaces are co-aligned on x and y (Fig. 5), only differing by a vertical offset. The linear solution for the fore, mid and aft beam offsets is found after reversing the transformation in Eq. (3):

$$\Delta\sigma^0_{fore} = (\Delta x + \Delta y)/\sqrt{2}$$
$$\Delta\sigma^0_{aft} = (\Delta x - \Delta y)/\sqrt{2}$$
$$\Delta\sigma^0_{mid} = \Delta z \quad (7)$$

If the relation between the cones were strictly linear, then the branch residuals after the optimal linear cone shift would be realizations of a spatially homogeneous random field with zero mean. The presence of structure in branch residuals after the linear correction, which should be carefully monitored, may uncover discrepancies in wind cone shapes that are constitutive of beam non-linearity.

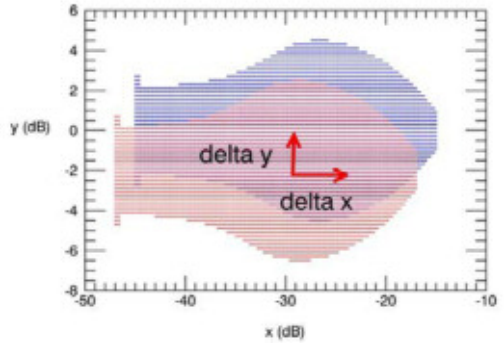

Fig. 5. Minimizing the RMS difference of the cone branch residuals for variable x and y coordinate shifts $\{\Delta x, \Delta y\}$.

C. Corrections to observation geometry

Changes in observation geometry due to variability in satellite attitude may induce changes in the observed backscatter distributions of up to 0.1 dB per 0.1 deg change in incidence. To separate geometric variability from other calibration effects, every backscatter measurement is to be geo-corrected to certain reference observation geometry (θ_0, ϕ_0) defined by the average incidence and azimuth angles obtained as a function of beam and node over the reference period, using a geophysical model function σ^0_{sim} (e.g. CMOD6) and scatterometer winds $\boldsymbol{v}_{scat}$ as:

$$\sigma = \sigma^0_{obs} + \sigma^0_{sim}(\vec{v}_{scat}, \theta, \phi) - \sigma^0_{sim}(\vec{v}_{scat}, \theta_0, \phi_0)$$

Where (θ,ϕ) are the actual incidence and azimuth angles of that particular backscatter point. Note that the geo-correction is applied in dB space.

While secular variations in incidence angle over the ASCAT period are generally less than 0.01 degrees, there is a remarkable gap in incidence angle between the ERS and ASCAT nodes (see Table I). The ERS nodes that have a direct correspondence with an ASCAT node (i.e. ERS nodes 5 to 18, in relation to ASCAT nodes 0 to 13) are geo-corrected to the geometry of the closest ASCAT node (up to 0.7 degrees away in incidence) as described above. Because the accuracy of the geo-correction degrades rapidly, the ERS nodes that lie outside of the ASCAT swath (i.e. ERS nodes 0 to 4 located between 2 and 11 degrees away in incidence from the closest ASCAT node) need special treatment and their analysis is deferred to future work.

To quantify the accuracy of the geo-correction, we analyze the residuals that arise between an actual ASCAT wind cone and one that has been geo-corrected from a neighbor node, as the node distance increases. We find that geo-correction errors increase RMS residuals by about 10% per degree change in incidence, with emerging residual structures that resemble those between the ASCAT wind cone and the GMF. Mark that the geo-correction bypasses the necessity of aligning the ERS and ASCAT node geometries at L1 level. The accuracy of the GMF-based geo-correction is limited by the imperfect match between the GMF and the actual data, although it generally affords good enough corrections for shifts in incidence angle of up to 1 degree.

D. Datasets

Maximum density surfaces have been drawn for a number of test datasets with a view towards their comparison, namely, ERS-1 over 1995, ERS-2 over 1997 and ASCAT-A over 2009. All of them are to be referenced against ASCAT-A data collected over 2013, which is taken as the reference dataset. The surfaces of maximum backscatter density are estimated using 50 km resolution (25 km grid) data.

1) ASCAT 2013

The reference cone is defined by ASCAT-A data collected from Jan 1st 2013 to Dec 31st 2013. These data have been reprocessed by EUMETSAT using L1B software version 9.01 and the latest calibration tables [12, 13]. The dataset is complemented by scatterometer winds (stress equivalent U10S) from the KNMI wind processor (AWDP) and model winds from the ECMWF operational NWP analyses.

2) ASCAT 2009

This dataset contains ASCAT-A data collected from Sep 1st 2008 to Aug 1st 2009. The backscatter data were processed by EUMETSAT using different L1B software versions and later aligned to software version 7.02 [8] with a focus on CMOD6 development. It is accompanied by scatterometer winds (neutral equivalent U10N) from the KNMI wind processor (AWDP) and model winds from the ECMWF operational NWP analyses.

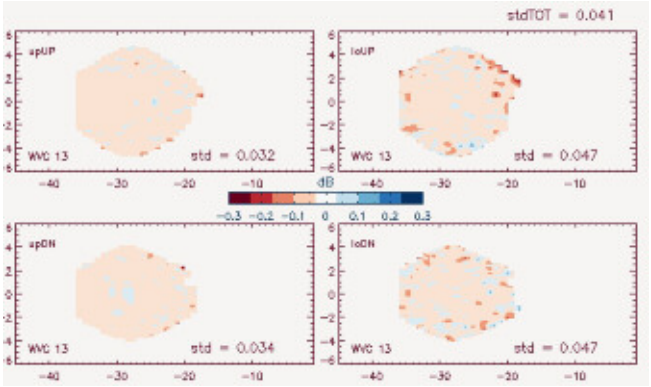

Fig. 7. Cone branch residuals between the ASCAT 2009 and ASCAT 2013 datasets (ASCAT WVC 13, right side) after linear shift correction. In the upper right corner, the RMS of the cone shape fit.

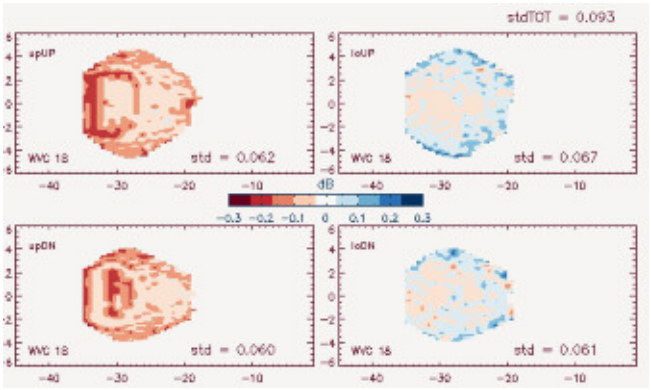

Fig. 8. Cone branch residuals between the ERS-1 1995 and ASCAT 2013 datasets (ERS WVC 18).

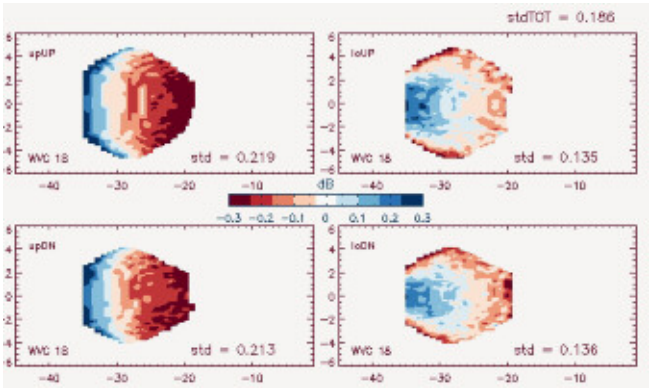

Fig. 9. Cone branch residuals between the ERS-2 1997 and ASCAT 2013 datasets (ERS WVC 18).

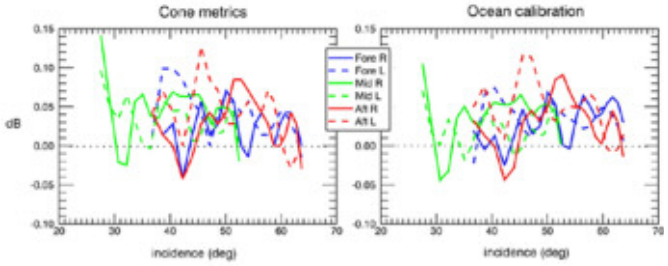

Fig. 6. Linear beam offsets between the ASCAT 2009 and ASCAT 2013 datasets: from cone metrics (left panel) and ocean calibration (right panel).

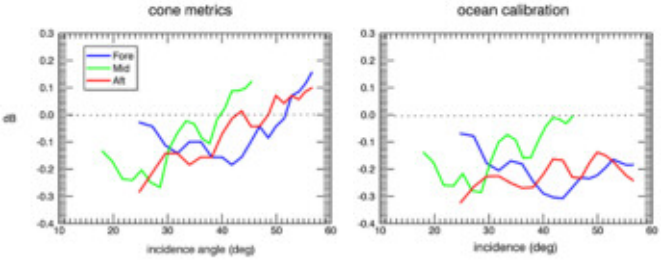

Fig. 10. Linear beam offsets between the ERS-2 1997 and ERS-1 1995 datasets: from cone metrics (left panel) and ocean calibration (right panel).

3) ERS-1 1995

This dataset comprises original ERS-1 data collected from Jan 1st 1995 to Dec 31st 1995 generated by the LRDPF processor [14] and retrieved from ECMWF MARS. It comes with scatterometer winds (U10N) from the KNMI wind processor (ESDP) and model winds from ERA40.

4) ERS-2 1997

This dataset comprises original ERS-2 data collected from Jan 1st 1997 to Dec 31st 1997 as generated by the LRDPF processor [14] and retrieved from ECMWF MARS. It comes with scatterometer winds (U10N) from the KNMI wind processor (ESDP) and model winds from ERA40.

III. Results and Discussion

A preliminary study based on simulation (not shown) proves that the cone shapes determined by cone metrics are insensitive to instrumental noise levels (Kp), geometric variability (i.e. dispersion around the mean observation angles) or the wind distribution of the underlying backscatter data, procuring estimates of linear beam offset with an accuracy of 0.02 dB. An illustration of the actual agreement in the determination of the relative linear beam offset between the ASCAT 2009 and ASCAT 2013 records from cone metrics and the ocean calibration method is shown in Figure 6, featuring an RMS difference of 0.015 dB (1σ). These linear offsets arise from the L1B processor upgrades from version 7.02 to version 9.01. The associated cone branch residuals are shown in Figure 7 as color-coded surfaces, attesting to their spatial homogeneity (RMS differences of 0.04 dB) and the concomitant stability of the reference ASCAT cone shape.

In contrast, the cone residuals for the ERS-1 and the ERS-2 datasets, both relative to the ASCAT 2013 dataset and shown in Figs. 8 and 9 as color-coded-surfaces, carry remarkable structures (particularly large for ERS-2) arising from dissimilarities between the ERS and ASCAT cone shapes. Structures in the branch residuals (RMS differences of up to 0.1 dB for the ERS-1 and 0.2 dB for the ERS-2 case, see Table II) prevent the cones from aligning properly and introduce incidence-dependent biases (of up to 0.3 dB) in the estimation of the linear beam offsets (see Figure 10). Removing the structure in ERS cone residuals calls for the introduction of backscatter-dependent calibration curves in the beams, as described in the next subsection.

Other than homogenizing the C-band backscatter record, cone metrics may target other applications. Figure 11 shows the cone branch residuals between the reference ASCAT 2013 cone and the CMOD6 geophysical model function (GMF) as color-coded surfaces, featuring residual RMS cone differences up to 0.3 dB. Residuals from cone metrics quantify the discrepancies between the model surface and the actual backscatter distributions, and suggest novel means towards improving the GMF.

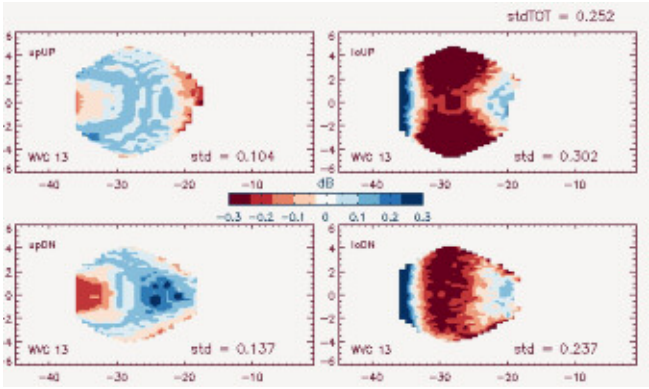

Fig. 11. Cone branch residuals between the ASCAT 2013 dataset and the CMOD6 geophysical model function (WVC 13).

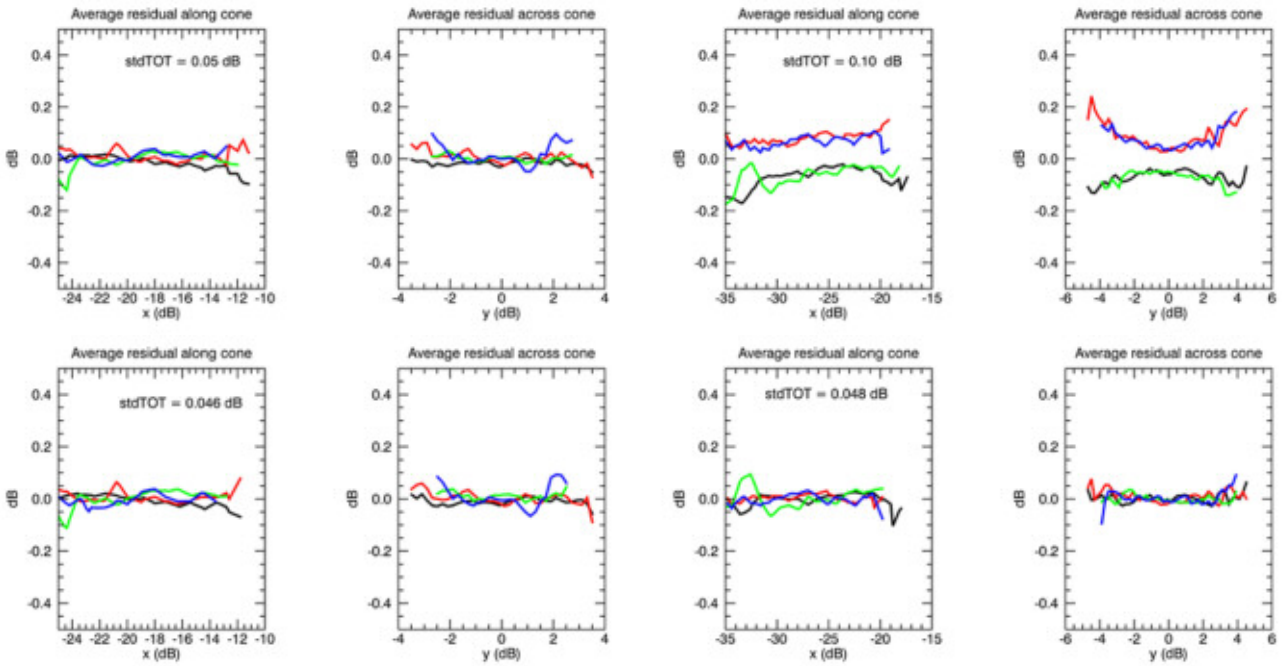

Fig. 12. Cone branch residuals between ERS-1 1995 and the ASCAT 2013 reference cone: before non-linear correction (top row) for WVC 5 (two left panels, first averaged across y, second averaged across x) and WVC 18 (two right panels); and after non-linear correction (bottom row) for WVC 5 (two left panels) and WVC 18 (two right panels). The cone branches are color-coded: upUP (black), loUP (red), upDN (green) and loDN (blue).

A. Non-linear corrections to ERS-1

After a series of trial an error runs put together in order to find a suitable function that removes the structure in the ERS cone residuals, we find that non-linearity in ERS-1 is consistent with a noise floor correction in the fore, mid and aft beams. The trial and error scheme consists on introducing a series of tentative (WVC-dependent) linear scaling factors α in the backscatter collected by each beam ($\sigma^0_{corr} = \alpha \cdot \sigma^0$), assuming for simplicity that the fore and aft beams are affected identically ($\alpha_{fore} = \alpha_{aft}$), to create a two-dimensional search space for the optimal (α_{mid}, α_{fore}) scaling factors that minimize the RMS difference to the reference cone. Plotting the optimal scaling factor solutions against the mean backscatter obtained for each node results in an exponential function, so that an exponential correction to backscatter is proposed for each beam and node as:

$$NFC(\sigma^0; N) = 10/\ln(10) \cdot 10^{-(\sigma^0 - N)/10} \quad (8)$$

Where σ^0 is backscatter in dB and N is a free fit parameter. Replacing the linear scaling approach by exponential curves is further verified by decreased RMS differences to the reference cone. Besides, the exponential curve in Eq. (8) may be optionally interpreted as a noise floor correction, where *N* is the noise floor term in dB, that would correspond to a small additive offset of $10^{N/10}$ to backscatter in linear space. The non-linear correction of Eq.(8) is applied ERS-1 backscatter in dB space as:

$$\sigma^0_{corr} = \sigma^0 - NFC(\sigma^0; N) \quad (9)$$

The node and beam dependent N parameters are determined by minimizing the RMS difference in cone residuals using a limited space of tentative {N_{mid}, $N_{fore/aft}$} combinations. Note that fore and aft beams are assumed to bear identical effects. The minimization of RMS residuals is performed over maximum density surfaces, which are typically defined for winds larger than 5 m/s. Over the low wind domain, the effect of the non-linear correction is verified by monitoring the behavior of the ERS tail histogram, that is, the frequency distribution of the lowest 2% of backscatter values, by requiring that it does not deviate from the reference ASCAT distribution. A sample analysis is presented in Fig.13 for WVC 15, showing that most of the correction in the low wind domain is carried by the ERS-1 fore and aft beams, and verifying the overall integrity of the noise floor subtraction hypothesis.

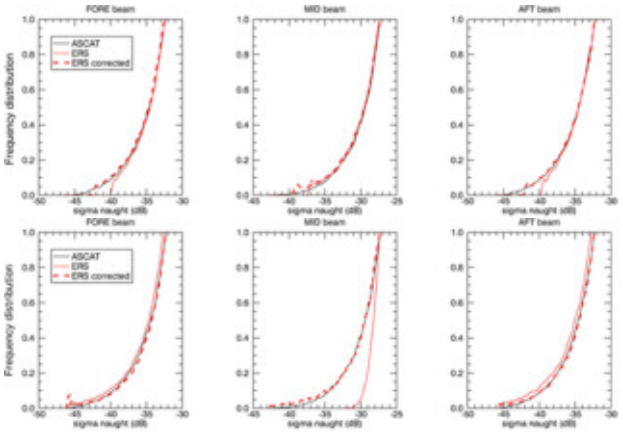

Fig. 13. Tail histograms for ERS WVC 15: frequency distributions of the lowest 2% of backscatter observations (scaled to unit peak value) before and after the non-linear correction, along with the reference ASCAT distribution (in black) for the fore (left), mid (middle) and aft (right) beams from ERS-1 (top row) and ERS-2 (bottom row).

At low incidence angles (where backscatter is stronger), the sensitivity to noise floor subtraction is reduced and the search for an optimal combination of non-linear parameters based on wind cone RMS differences returns very wide minima. In these cases, tail histograms are used to constrain the search problem by requiring that an optimal solution be found that also minimizes the variance between the ERS and ASCAT tail histograms. Eventually, the optimal {N_{mid}, $N_{fore/aft}$} solutions achieve the largest cone fit improvements at large incidence nodes (see Table II) and effectively remove any structure left in the branch residuals (see also Fig. 12), leaving the cones aligned and ready for the estimation of the linear beam offsets.

TABLE II
ERS NON-LINEAR CORRECTION PARAMETERS AND RMS FIT

ERS WVC	ERS-1 N MID	ERS-1 N FORE/AFT	ERS-1 RMS FIT*	ERS-2 N MID	ERS-2 N FORE/AFT	ERS-2 RMS FIT*
5	-55 dB	-55 dB	0.051/0.046	-25 dB	-50 dB	0.065/0.052
6	-55 dB	-55 dB	0.052/0.046	-25 dB	-50 dB	0.059/0.052
7	-55 dB	-45 dB	0.051/0.045	-25 dB	-52.5dB	0.062/0.048
8	-55 dB	-44 dB	0.054/0.048	-25 dB	-52.5dB	0.074/0.048
9	-55 dB	-45 dB	0.055/0.049	-25.5dB	-50 dB	0.087/0.051
10	-55 dB	-44 dB	0.060/0.053	-26 dB	-50 dB	0.096/0.051
11	-55 dB	-44 dB	0.062/0.051	-26.5dB	-47.5dB	0.102/0.056
12	-55 dB	-43 dB	0.061/0.054	-27 dB	-50 dB	0.096/0.050
13	-44 dB	-43 dB	0.061/0.053	-27.5dB	-52.5dB	0.101/0.052
14	-43 dB	-42 dB	0.064/0.056	-28 dB	-52.5dB	0.104/0.053
15	-40 dB	-42 dB	0.067/0.052	-28 dB	-50 dB	0.129/0.049
16	-39 dB	-40 dB	0.078/0.056	-28 dB	-50 dB	0.136/0.050
17	-39 dB	-39 dB	0.079/0.055	-28 dB	-47.5dB	0.165/0.058
18	-38 dB	-37 dB	0.094/0.050	-28 dB	-47.5dB	0.182/0.061

* The RMS fit refers to the RMS difference in cone residuals before/after the non-linear correction.

B. Non-linear corrections to ERS-2

The principle behind the formulation of non-linear corrections is the search for minimum RMS differences to the reference ASCAT cone. The noise floor subtraction proposed for ERS-1 does not work well in the ERS-2 case for two reasons. Firstly, matching the cone shapes in the ERS-1 case led us to the subtraction of noise floor components in the fore, aft and mid beams. In the ERS-2 case, the RMS differences to the reference cone decrease when the noise floor corrections in Eq. (8) are added to the fore/aft beams, instead of subtracted. This raises questions as to which aspects of the L1B processor or specific scatterometer settings changed between the ERS-1 and ERS-2 records, their instrumental designs being otherwise identical. Secondly, the ERS-2 cones are fit properly using the ERS-1 noise floor corrections in Eq. (8) for winds larger than 5 m/s, yet the analysis of tail histograms (not shown) indicates that these corrections are adding too much backscatter to the fore/aft beams, and subtracting too little from the mid beam in the low wind domain.

To fix this problem, the shape of the ERS-1 noise floor correction has to be modified so as to provide a better fit to the

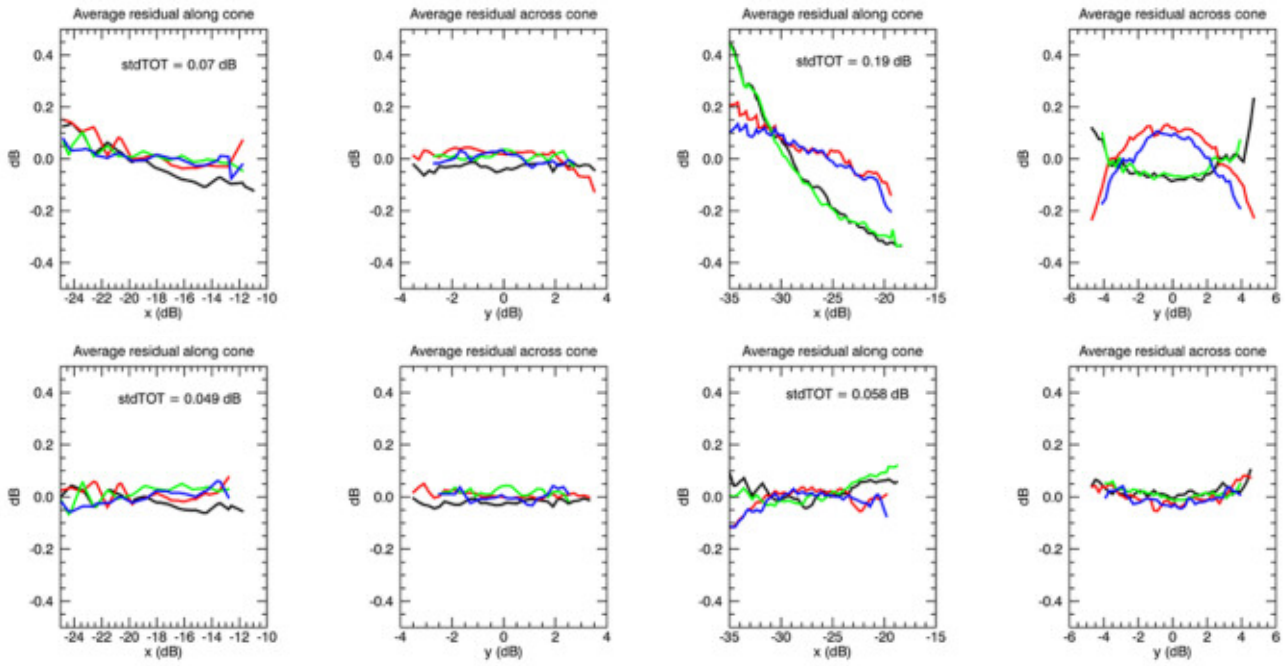

Fig. 15. Same as Fig.12 but for ERS-2 1997.

reference tail histograms. The following node- and beam-dependent calibration curves are proposed for ERS-2:

$$NFC_{fore/aft}(\sigma^0;N) = 10/\ln(10)\cdot 10^{-(\sigma^0-N)/25} \quad (10)$$

$$NFC_{mid}(\sigma^0;N) = 10/\ln(10)\cdot(10^{-(\sigma^0-N)/7} + 10^{-(\sigma^0-N)/3}) \quad (11)$$

where we force a steeper slope to the non-linear correction at low SNR for the mid beam, and a more gentle slope for the fore and aft beams. Figure 14 shows a comparison between the noise floor correction curve for ERS-1 in Eq.(8), and the modified non-linear correction curves for the ERS-2 side [Eq.(10)] and mid beams [Eq.(11)] as a function of SNR, the latter defined as σ^0-N (in dB). As with ERS-1, the optimal $\{N_{mid}, N_{fore/aft}\}$ solutions are determined by minimizing the RMS difference in cone residuals, and using the variance between the ERS and ASCAT tail histograms to constrain the search. The optimal non-linear correction parameters (see Table II) bring about the largest cone fit improvements at the largest node numbers, though they can still be felt at low incidences, and are overall successful at removing any structure left in the cone branch residuals (see also Fig. 15). The analysis of the ERS-2 tail histograms in Fig. 13 shows that most of the correction in the low wind domain is carried by the mid beam, and verifies that it actually brings the ERS-2 tail histograms closer to the ASCAT reference, as desired.

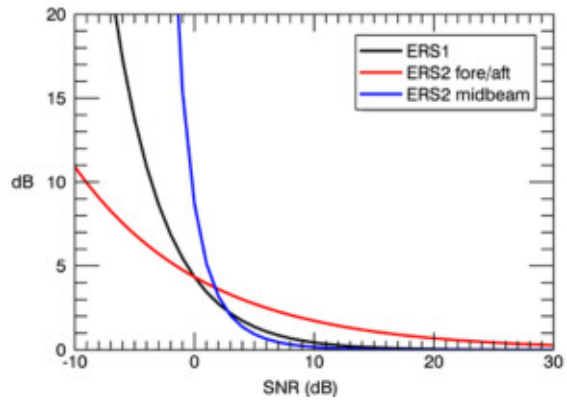

Fig. 14. Non-linear correction curves for ERS-1 and ERS-2: in black, the ERS-1 noise floor function in Eq.(8). Overlaid, the modified ERS-2 non-linear correction curves for the fore/aft beams (red) in Eq. (10) and mid beam (blue) in Eq.(11). The SNR refers to (σ^0-N), both expressed in dB.

IV. Summary and Conclusion

We have described a novel method for the inter-calibration of the C-band scatterometer record, termed cone metrics, which is based on monitoring changes in the location and shape of the maximum density surface of ocean backscatter measurements. Using cone metrics, we have established the linear and non-linear corrections necessary to homogenize the ERS-1, ERS-2 and ASCAT records down to 0.05 dB.

It is known that the ocean backscatter points collected at C-band are distributed along a double-folded conical surface in the scatterometer measurement space, also known as the wind cone. The basic principle of cone metrics holds that ocean backscatter points collected under identical observation angles must conform to the same wind cone. Inconsistencies between the backscatter distributions observed by different instruments over different periods may be attributed to relative beam calibration biases (that shift the location of the wind cone) or beam non-linearities (which cause the wind cone to deform).

Cone metrics results indicate that the shape of the wind cone does not change significantly over the ASCAT period, featuring residual RMS cone differences of 0.04 dB, which is a necessary condition for the assumption of linear beam offset to hold. Over the ASCAT period, the linear beam offsets derived from cone metrics have been validated against ocean calibration to an accuracy of 0.02 dB.

A preliminary analysis based on simulation demonstrates

that the wind cone shapes determined by cone metrics are not sensitive to random instrumental noise levels, geometric variability or changes in the input wind distribution, all of which is required in order to export the ASCAT reference cone to ERS conditions. Connecting to the ERS period must also account for changes in the mean node observation angles: geometrical corrections have been devised to bring the ERS nodes in line with the ASCAT nodes that lie the closest (up to 0.7 degrees away in incidence). Because the accuracy of the geo-correction degrades rapidly, the ERS nodes that lie outside of the ASCAT swath (i.e., ERS nodes 0 to 4, up to 10 degrees away in incidence) need special treatment and their analysis is deferred to future work.

Aligning the ERS-1 and ERS-2 records to the ASCAT reference cone is made difficult by the presence of systematic structures in the wind cone residuals, indicating that the ERS and ASCAT records are related non-linearly. The residual RMS cone differences amount to 0.1 dB for ERS-1 and 0.2 dB for ERS-2, typically increasing with incidence and calling for the introduction of backscatter-dependent corrections in the beams. After a series of trial an error runs, we find that non-linearity in ERS-1 is removed after subtraction of a combination of noise floor corrections in the fore, mid and aft beams. The beam- and node-dependent noise floor parameters are obtained after minimization of the RMS difference of cone residuals. The non-linear correction for ERS-2 differs from that applied to ERS-1 in two aspects: on one hand, the fore and aft beams demand addition of noise floor corrections, on the other hand, the noise floor corrections must be modified somewhat in order to match the reference backscatter distributions at low winds. The origin of the ERS non-linearities and the reason why the ERS-1 and ERS-2 records require such different treatment should be subject to future work. In any case, the non-linear corrections proposed here bring the ERS-1 and ERS-2 wind cone shapes back in line with the ASCAT reference cone, featuring residual RMS cone differences of 0.05 dB. This corresponds to wind speed differences of approximately 0.05 m/s, well in compliance with the GCOS requirement for the provision of a climate data record of ocean surface wind speeds. A reprocessing of the entire ERS dataset, using the non-linear corrections proposed here, is planned, along with an analysis of their impact on the winds retrieved. To fully understand the ERS climate record, it would be advisable to trace these corrections back to specific settings in the ERS instruments or conversion steps in the L1B processor.

Other than homogenizing the C-band scatterometer record, cone metrics may also be used to evaluate the agreement between the geophysical model functions used for wind retrieval and the actual backscatter distributions. For example, the residual RMS cone differences between the CMOD6 and the reference ASCAT 2013 cone amount to 0.3 dB, suggesting novel means towards improving the GMF beyond CMOD7 [15].

ACKNOWLEDGMENTS

The authors would like to thank ESA, EUMETSAT and ECMWF for the data provided. The results described in this manuscript were obtained in the ESA SCIROCCO project.

REFERENCES

[1] Bentamy, A., Grodsky, S., Elyouncha, A., Chapron, B., Desbiolles, F., "Homogenization of scatterometer wind retrievals", Int. J. Climatol., doi:10.1002/joc.4746, 2016.

[2] Wang, Z., Stoffelen, A., Fois, F., Verhoef, A., Zhao, C., Lin, M., Chen, G, "SST dependence of Ku- and C-band backscatter measurements", to appear in this issue, 2016.

[3] Figa-Saldana, J., Wilson, J.J.W., Attema, E., Gelsthorpe, R., Drinkwater, M.R., Stoffelen, A., "The advanced scatterometer (ASCAT) on the meteorological operational (MetOp) platform: A follow-on for European wind scatterometers", Can. J. Remote Sensing, Vol. 28, No. 3, pp. 404-414, 2002.

[4] Attema, E.P.W., "The active microwave instrument (AMI) on-board the ERS-1 satellite", Proc. IEEE, Vol. 79, No. 6, pp. 791-799, Jun. 1991.

[5] WMO (World Meteorological Organization), "Systematic observation requirements for satellite-based data products for climate", Report GCOS-154, 128 pp., Geneva, Switzerland, 2011.

[6] Manise, N., Neyt, X., Acheroy, M., "Calibration strategy for ERS scatterometer data reprocessing", Proc. SPIE 5977, Remote Sensing of the Ocean, Sea Ice and Large Water Regions, doi:10.1117/12.627708, 2005.

[7] Wilson, J.J.W., Anderson, C., Baker, M.A., Bonekamp, H., Figa-Saldana, J., Dyer, R.G., Lerch, J.A., Kayal, G., Gelsthorpe, R.V., Brown, M.A., Schied, E., Schutz-Munz, S., Rostan, F., Pritchard, E.W., Wright, N.G., King, D., Onel, U., "Radiometric calibration of the Advanced Wind Scatterometer radar ASCAT carried onboard the METOP-A satellite", *IEEE Trans. Geosci. Rem. Sens.*, vol. 48, no. 8, pp. 3236–3255, Aug. 2010.

[8] J. Verspeek, "Improved ASCAT wind retrieval using NWP Ocean Calibration," *IEEE Trans. Geosci. Rem. Sens.*, vol. 50, no. 7, pp. 2488–2498, Feb. 2012.

[9] Long, D.G., Skouson, G.B., "Calibration of spaceborne scatterometers using tropical rain forests", *IEEE Trans. Geosci. Rem. Sens.*, vol. 34, no. 2, pp. 413–424, Mar. 1996.

[10] Anderson, C., Bonekamp, H., Figa, J., Wilson, J.J.W., "Monitoring ASCAT-A calibration using ocean backscatter", Poster presented at the International Ocean Wind Vector Science Team (IOWVST) meeting in Utrecht, The Netherlands, 2012.

[11] Stoffelen, A., Anderson, D., "Scatterometer data interpretation: measurement space and inversion", J. Atmos. Ocean. Tech, 14(6), pp 1298-1313, 1997.

[12] EUMETSAT, "Metop-A ASCAT L1 Data Record Release 2 (CF-003): User guide", EUM/OPS-EPS/USR/14/739701, 2014.

[13] EUMETSAT, "Metop-A ASCAT L1 Data Record Release 2 (CF-003): Validation Report", EUM/TSS/REP/14/753112, 2014.

[14] Lecomte, P., "ERS wind product specifications", Proc. ESA/EUMETSAT Workshop, Noordwijk, 5-7 October 1998. Available: https://earth.esa.int/pub/ESA_DOC/scatt_work98_product.pdf.

[15] Stoffelen, A., Verspeek, J., Vogelzang, J., Verhoef, A., "The CMOD7 geophysical model function for ASCAT and ERS retrievals", this issue (submitted as JSTARS-2016-01224).

Maria Belmonte Rivas received her B.Sc. degree in earth sciences from the Universidad Complutense de Madrid, Spain in 1999 and the M.Sc. and Ph.D. degrees in physics and aerospace engineering from the University of Colorado in Boulder in 2007.

In her previous appointments at the European Space Agency (ESTEC, The Netherlands), the University of Colorado in Boulder (USA), the Atmospheric

Chemistry Division at the National Center for Atmospheric Research (NCAR, USA), and the Technical University of Delft (The Netherlands), she has been involved in the development of satellite remote sensing techniques for Earth Observation. She has contributed to the analysis of Global Positioning System signals for the monitoring of ocean heights, ocean winds and polar sea ice. She has developed sea ice detection algorithms for scatterometers like Quikscat and ASCAT, and contributed to the retrieval of stratospheric trace gas profiles from infrared limb sounders like HIRDLS, or tropospheric NO_2 profiles for nadir spectrometers like OMI.

Ad Stoffelen leads a group on satellite active remote sensing for meteorological applications and is involved in topics from future missions and retrieval to 24/7 operations, user training and services. He is also deeply involved in the European Space Agency ADM-Aeolus Doppler Wind Lidar mission.

Jeroen Vespeek was born in 1962, in The Netherlands. He received his M.Sc. degree in physics from the Technical University of Eindhoven, Eindhoven, The Netherlands, in 1988.
He is currently with the Royral Netherlands Meteorological Institute (KNMI), De Bilt, The Netherlands, and is working on GMF development, scatterometer data interpretation, inversion, calibration, validation and quality monitoring..

Anton Verhoef was born in 1964 in The Netherlands. He received his M.Sc. degree in physics from the Rijksuniversiteit Groningen, The Netherlands in 1989 and his Ph.D in Solid State Physics at the Rijksuniversiteit Groningen in 1994.
He is currently with the Royal Netherlands Meteorological Institute (KNMI) and working on scatterometry processing software development, data validation, quality monitoring and user services.

Xavier Neyt received a master in engineering (summa cum laude) from the Université Libre de Bruxelles (ULB) in 1994, a postgraduate degree in Signal Processing (summa cum laude) from the Université de Liège (ULg) in 2004 and a PhD in Applied Science from the Royal Military Academy (RMA) and the Université de Liège in 2008. In 1995 he received the Frerichs Award from the ULB and the special IBM grant from the Belgian National Fund for Scientific Research (NFWO).
He has been working as research engineer for the Royal Military Academy, Belgium. In 1996-1997 he was visiting scientist at the French aerospace center (ONERA) and in 1999 at the German aerospace centre (DLR). In 1997-1999 he was responsible for the design of the image compression module of the European MSG satellite and in 2000-2007, responsible for the redesign of the ground processing of the scatterometer of the European ERS satellite following its gyroscope anomaly. Since 2008, he is leading the Scatterometer Engineering Support Laboratory for the European Space Agency at the Royal Military Academy.
Mr. Neyt is associate professor at the Communication, Information, Systems and Sensors department of the Royal Military Academy. His research interests are signal processing, radar remote sensing, array processing, bistatic radars and image processing

Craig Anderson received a BSc (Honours) in applied mathematics and a PhD in theoretical solar physics from St Andrews University in Scotland. He worked for several years in the Marconi Research Centre in England developing applications for airborne and spaceborne synthetic aperture radars before joining EUMETSAT in Darmstadt, Germany. For the last 10 years he has been involved in the calibration and validation of the Advanced Scatterometers (ASCAT) on the Metop-A and Metop-B satellites.